2021 43rd Annual International Conference of the
IEEE Engineering in Medicine & Biology Society (EMBC)
Oct 31 - Nov 4, 2021. Virtual Conference

PPG-Based Respiratory Rate Monitoring Using Hybrid Vote-Aggregate Fusion Technique

Serj Haddad, Assim Boukhayma, and Antonino Caizzone

Abstract— **In this work, we present a low-complexity photoplethysmography-based respiratory rate monitoring (PPG-RRM) algorithm that achieves high accuracy through a novel fusion method. The proposed technique extracts three respiratory-induced variation signals, namely the maximum slope, the amplitude, and the frequency, from the PPG signal. The variation signals undergo time domain peak detection to identify the inter-breath intervals and produce three different instantaneous respiratory rate (IRR) estimates. The IRR estimates are combined through a hybrid vote-aggregate fusion scheme to generate the final RR estimate. We utilize the publicly available Capnobase data-sets [1] that contain both PPG and capnography signals to evaluate our RR monitoring algorithm. Compared to the reference capnography IRR, the proposed PPG-RRM algorithm achieves a mean absolute error (MAE) of** 1.44 **breaths per minute (bpm), a mean error (ME) of** 0.70 ± 2.54 **bpm, a root mean square error (RMSE) of** 2.63 **bpm, and a Pearson correlation coefficient** $r = 0.95$**,** $p < .001$**.**

I. Introduction

The number of breaths per minute, known as respiratory or respiration rate (RR), is a vital clinical sign that provides significant information regarding the ventilation in the human body. Changes in the RR parameter often constitute the first signs of decline in patient status and deterioration of the body as it attempts to maintain oxygen supply to the cells. With the COVID-19 outbreak, RR monitoring among individuals became of utmost importance for early detection of positive cases. Recently, a model which relies on the RR variation during night-time sleep to estimate the probability of SARS-CoV-2 infection was proposed. The given model was capable of tracking 20% of the COVID-19 positive individuals in the two days prior to the symptom onset, and 80% of the COVID-19 positive cases by the third day of symptoms [2]. Therefore, it goes without saying that continuous RR monitoring is essential for early detection and intervention.

Many of the RR monitoring methods are obtrusive and cause discomfort for patients, especially when the RR tracing is done continuously for long periods of time. For this reason, Photoplethysmography (PPG) was proposed as a promising low-cost, non-invasive, and non-occlusive technique for instantaneous respiratory rate (IRR) estimation. PPG involves using a light-emitting diode (LED) to illuminate the skin and measuring the intensity of either the transmitted or the reflected light to a photo-diode. This optical solution tracks the variation in the blood volume. It is already widely deployed in smart watches, many smart phones, and different wearable devices. Studies confirm the accuracy of PPG-based solutions to monitor different vital signs and physiological signals, such as heart rate (HR) and heart rate variability (HRV) [3], [4], systolic and diastolic blood pressure variation [5], [6], irregularity in heart beats [7], [8], stress levels [9], [10], quality of sleep [11], etc.

PPG-based solutions can be provided to the widest possible population, enabling continuous long-term RR monitoring with acceptable accuracy. A variety of methods have been developed for IRR estimation from a PPG signal [1], [12]–[15]. These methods involve diverse time and frequency domain signal processing techniques, such as short-time Fourier Transform, different time-frequency synchrosqueezing techniques, empirical mode decomposition, etc. In this work, we present a temporal signal processing technique that has low-complexity, which is essential for real-time RR monitoring, and acceptable accuracy.

The paper is organized as follows. Section II presents the methods used for this study. This includes information about the Capnobase data-sets, the statistics of the acquired data, and the methods utilized to process them. Section III provides a detailed description of the PPG-RRM algorithm. Section IV evaluates the accuracy of the proposed scheme compared to the reference capnography data. Finally, Section V summarizes our conclusions.

II. Materials and Methods

We use the Capnobase test data-sets containing 42 8-min recordings with reference CO_2 waveforms (capnograms) and pulse oximetry finger PPG [1]. The 42 data-sets, 29 pediatric and 13 adults, contain recordings of spontaneous and controlled breathing.

The respiratory rate extracted from the capnography waveform is used as the reference gold standard. The recordings are divided into intervals of 3 seconds. For each 3-second window, a reference IRR value is assigned. In total, there are 5605 clean windows with reference IRR values. The statistics of these data points is summarized in Table I.

The metrics used to evaluate the accuracy of the proposed algorithm to estimate the respiratory rate are: mean error (ME, in bpm), standard deviation of error (SDE, in bpm), mean absolute error (MAE, in bpm), root mean square error (RMSE, in bpm), and the Pearson correlation coefficient r.

III. Algorithm

In this section, we present the PPG-RRM algorithm, illustrated in Fig. 3 in the form of a block diagram.

All authors (corresponding author: serj.haddad@senbiosys.com) are with Senbiosys SA, Neuchâtel, Switzerland.

TABLE I

THE STATISTICS OF THE CAPNOGRAPHY REFERENCE IRR DATA.

Number of Data Points	5605
Mean (bpm)	15.14
Standard deviation (bpm)	7.61
Range (bpm)	3.46-45.32

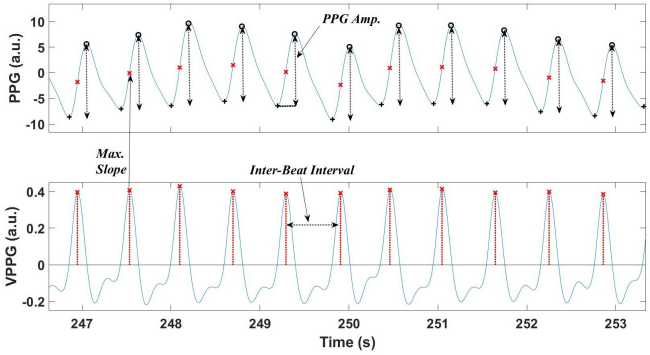

Fig. 1. The upper plot shows the PPG signal with the identified peaks and troughs used to compute the PPG amplitude values. The lower plot shows the VPPG signal with the identified peaks used to compute the maximum slope values and the inter-beat intervals.

A. Beat and Amplitude Detection

The beat and amplitude detection sub-block implements the beat-to-beat detection algorithm presented in [4] on input PPG signal to identify the PPG pulses. The inter-beat interval detection is based on identifying the peaks of the 1st derivative of the PPG signal, known as the velocity PPG (VPGG), as shown in the lower plot of Fig. 1. The identified points represent the maximum slope of the PPG pulse. The maximum and the minimum values between the consecutive maximum slope points represent the peaks and the troughs of the PPG signal, as shown in the upper plot of Fig. 1.

B. Generate Respiratory Induced Signals

The characteristic points detected by the *beat and amplitude detection* sub-block are used to generate three respiratory induced variation signals.

1) Respiratory Induced Maximum Slope Variation (RIMSV): It is the change in the peak values of the VPPG signal. These values are resampled at 4 Hz and band-pass filtered with cutoff frequencies of 0.067 Hz and 1 Hz (corresponding to breathing rate values between 4 and 60 bpm). The filtered signal then undergoes peak detection, as shown in the first plot of Fig. 2, to compute the inter-breath interval values that are stored in the RR MSV buffer.

2) Respiratory Induced Amplitude Variation (RIAV): It is the variation in the amplitude of the PPG signal obtained by computing the difference between the PPG peak values and their corresponding trough values (refer to the upper plot in Fig. 1). These values are resampled at 4 Hz and band-pass filtered. The obtained signal then undergoes peak detection, as shown in the second plot of Fig. 2, to compute the inter-breath interval values that are stored in the RR AV buffer.

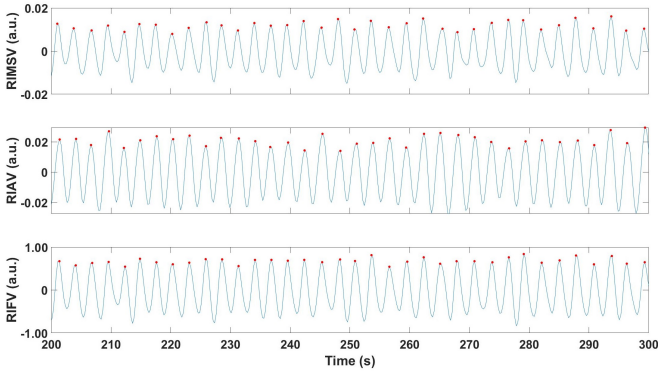

Fig. 2. The generated respiratory-induced maximum slope, amplitude, and frequency variation signals used to compute the inter-breath intervals through peak detection.

3) Respiratory Induced Frequency Variation (RIFV): It is the frequency variation of the VPPG signal generated using the inter-beat interval values, which are the intervals between the consecutive VPPG peaks (refer to the lower plot in Fig. 1). These values are resampled at 4 Hz and band-pass filtered. The resulting signal then undergoes peak detection, as shown in the third plot of Fig. 2, to compute the inter-breath interval values that are stored in the RR FV buffer.

C. Hybrid Vote-Aggregate Fusion

The three RR buffers/queues are fed into the final sub-block of our algorithm, namely the *Fuse* sub-block (see Fig. 3). This block implements the *hybrid vote-aggregate fusion* algorithm. The proposed fusion algorithm either aggregates two of the three RR estimates or votes for one of the three based on the median and the standard deviation of the three RR vectors. An overview of the proposed algorithm is presented in **Algorithm 1** as a pseudo-code.

1) Aggregate Fuse: if the absolute difference between the medians of the FV and the MSV RR vectors is below a certain threshold, then we *aggregate* the two medians by setting the final RR estimate to their mean value. Otherwise, if the absolute difference between the medians of the AV and the MSV RR vectors is below a certain threshold, then we *aggregate* the two medians by setting the final RR estimate to their mean value. Finally, if both mentioned conditions are not satisfied, we *vote* for either of the three median values.

Note that our solution first tries to aggregate between frequency-based (MED_{FV}) and amplitude-based (MED_{MSV}) RR estimates. If this fails, it tries to aggregate between two amplitude-based (MED_{MSV} and MED_{AV}) RR estimates.

2) Vote Fuse: the final RR estimate is set to the median of the RR vector that has the minimum standard deviation. Lower standard deviation indicates that the inter-breath interval values in the RR buffer are more uniform and stable.

IV. RESULTS

The performance of our proposed algorithm is summarized in Table II. In the same table, we show the performance of the Smart Fusion by Karlen *et al.* [1]. Both the proposed and the Smart Fusion methods show similar performance.

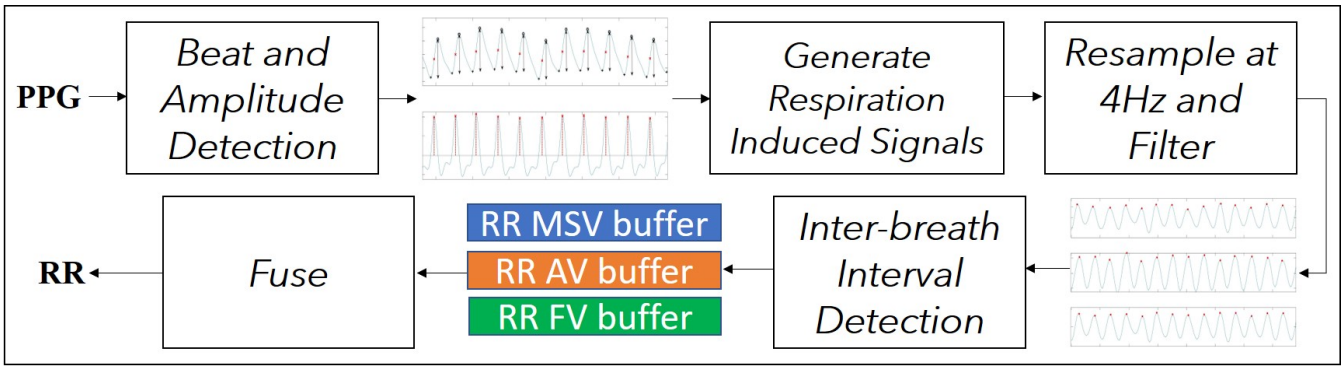

Fig. 3. The block diagram of the PPG-RRM algorithm: 1) Identifying the PPG peaks/troughs and the VPPG peaks, 2) generating the respiratory induced maximum slope, amplitude, and frequency variation signals, 3) processing the generated variation signals, 4) peak detection of the processed signals for inter-breath interval detection, and 5) Fusing the RR estimates.

Algorithm 1: hybrid vote-aggregate fusion algorithm

Input:
$RR_{FV}, RR_{MSV}, RR_{AV}$: respectively, Freq., Max. Slope, and Amp. based RR estimate vectors.
$Threshold$: used to decide whether to aggregate fuse or vote fuse.
Output:
RR_{Final}: Final respiration rate estimate.

```
VoteAggregateFusion(RR_FV, RR_MSV, RR_AV, Threshold)
MED_FV ← median{RR_FV}
MED_MSV ← median{RR_MSV}
MED_AV ← median{RR_AV}
σ_FV ← stdev{RR_FV}
σ_MSV ← stdev{RR_MSV}
σ_AV ← stdev{RR_AV(i1 : i2)}
if abs(MED_FV − MED_MSV) < Threshold then
    RR_Final ← (MED_FV + MED_MSV)/2
else
    if abs(MED_MSV − MED_AV) < Threshold then
        RR_Final ← (MED_MSV + MED_AV)/2
    else
        i ← arg min{σ_FV, σ_MSV, σ_AV}
        switch i do
            case 1 do
                RR_Final ← MED_FV
            end
            case 2 do
                RR_Final ← MED_MSV
            end
            case 3 do
                RR_Final ← MED_AV
            end
        end
    end
end
```

TABLE II
PERFORMANCE EVALUATION OF THE PPG-RRM ALGORITHM WITH RESPECT TO KARLEN *et al.*

	PPG-RRM	***Karlen et al.* [1]**
ME (bpm)	0.70	-0.63
SDE (bpm)	2.54	2.93
MAE (bpm)	1.44	1.19
RMSE (bpm)	2.63	2.99
Corr. Coef. r	0.95	0.93
Output Percentage (%)	100	55.36

Our proposed scheme achieves a slightly better performance in terms of SDE (2.54 bpm vs 2.93 bpm), RMSE (2.63 bpm vs 2.99 bpm), and correlation coefficient r (0.95 vs 0.93). On the other hand, the Smart Fusion technique achieves a better MAE (1.19 bpm vs 1.44 bpm). However, the main achievement of the PPG-RRM algorithm resides in maintaining a good performance with a 100% output rate. In other words, our method generates IRR estimates for all the 5605 reference IRR values. On the other hand, the Smart Fusion method maintains a good performance by discarding many of its IRR estimates, which results in an output rate of only 55.36% (only 3103 of the reference IRR values have corresponding IRR estimates). In Fig. 4, we demonstrate the number of RR estimates per subject generated by the PPG-RRM and the Karlen *et al.* algorithm. The plot shows that our proposed solution generates consistently ~ 140 RR estimates per subject. Note that due to the noisy capnography waveform, some subjects have less reference IRR data points.

In Fig. 5, we illustrate the high correlation between the PPG-based IRR estimates generated by the proposed algorithm and the corresponding capnography RR values (reference IRR) with an r value of 0.95, $p < .001$. We further present the Bland-Altman plot for the IRR estimates in Fig. 6 with the 95% limits of agreement ($\mu \pm 1.96\sigma$, where μ and σ denote the bias and the error standard deviation, respectively) from -4.28 bpm to 5.68 bpm.

V. CONCLUSION

In this work, we present the PPG-RRM algorithm based on hybrid vote-aggregate fusion approach for continuous

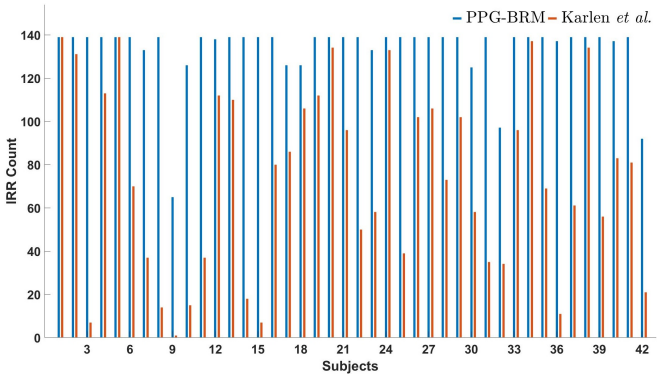

Fig. 4. The number of RR estimates generated by the PPG-RRM and the Karlen *et al.* algorithm for each of the 42 subjects.

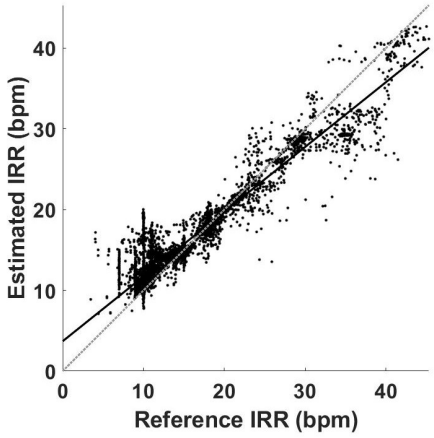

Fig. 5. The plot shows the high correlation between the estimated and the reference respiratory rate values; Pearson correlation coefficient $r = 0.95$, $p < .001$.

respiratory rate monitoring using PPG signal. The accuracy of the proposed algorithm is evaluated using the publicly available Capnobase test data-sets. The performance results obtained indicate that the proposed PPG-based RR monitoring solution is capable of accurately estimating the instantaneous respiratory rate with a 95% confidence interval $\mu \pm 1.96\sigma = \{-4.28, 5.68\}$ bpm, a mean absolute error of 1.44 bpm, a root mean square error of 2.63 bpm, and a Pearson correlation coefficient $r = 0.95$, $p < .001$.

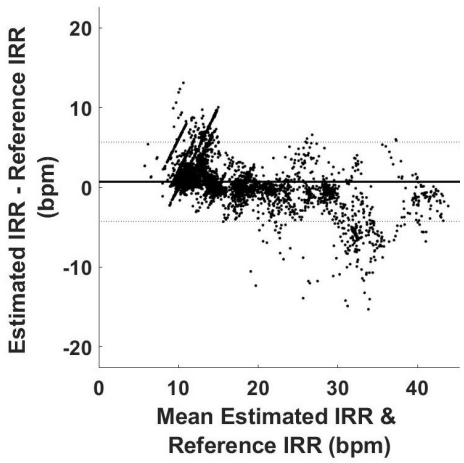

Fig. 6. Bland-Altman plot for IRR estimates shows the 95% confidence interval $\mu \pm 1.96\sigma = \{-4.28, 5.68\}$ bpm.

REFERENCES

[1] W. Karlen, S. Raman, J. M. Ansermino, and G. A. Dumont, "Multiparameter respiratory rate estimation from the photoplethysmogram," *IEEE Transactions on Biomedical Engineering*, vol. 60, no. 7, pp. 1946–1953, 2013.

[2] D. J. Miller, J. V. Capodilupo, M. Lastella, C. Sargent, G. D. Roach, V. H. Lee, and E. R. Capodilupo, "Analyzing changes in respiratory rate to predict the risk of covid-19 infection," *medRxiv*, 2020.

[3] U. R. Acharya, K. P. Joseph, N. Kannathal, C. M. Lim, and J. S. Suri, "Heart rate variability: a review," in *Medical & Biological Engineering & Computing*, vol. 44, pp. 1031–1051, 2006.

[4] S. Haddad, A. Boukhayma, and A. Caizzone, "Beat-to-beat detection accuracy using the ultra low power senbiosys ppg sensor," in *8th European Medical and Biological Engineering Conference (EMBEC 2020)*, pp. 178–188, Springer, 2020.

[5] A. D. Choudhury, R. Banerjee, A. Sinha, and S. Kundu, "Estimating blood pressure using windkessel model on photoplethysmogram," in *2014 36th Annual International Conference of the IEEE Engineering in Medicine and Biology Society*, pp. 4567–4570, 2014.

[6] S. Haddad, A. Boukhayma, and A. Caizzone, "Continuous ppg-based blood pressure monitoring using multi-linear regression," https://arxiv.org/abs/2011.02231.

[7] S. Haddad, J. Harju, A. Tarniceriu, T. Halkola, J. Parak, I. Korhonen, A. Yli-Hankala, and A. Vehkaoja, "Ectopic beat-detection from wrist optical signals for sinus rhythm and atrial fibrillation subjects," in *XV Mediterranean Conference on Medical and Biological Engineering and Computing – MEDICON*, pp. 150–158, September 2019.

[8] A. Tarniceriu, V. Vuohelainen, S. Haddad, T. Halkola, J. Parak, J. Laurikka, and A. Vehkaoja, "Performance of wrist photoplethysmography in monitoring atrial fibrillation in post cardiac surgery patients," in *2019 Computing in Cardiology (CinC)*, pp. 1–4, 2019.

[9] J. Sztajzel, "Heart rate variability: a noninvasive electrocardiographic method to measure the autonomic nervous system," vol. 134(35-36), pp. 514–522, Swiss Med Wkly, 2004.

[10] J. Thayer, F. Åhs, M. Fredrikson, J. J. Sollers III, and T. D. Wager, "A meta-analysis of heart rate variability and neuroimaging studies: implications for heart rate variability as a marker of stress and health," in *Neuroscience and Biobehavioral Reviews*, vol. 36(2), pp. 747–756, 2012.

[11] P. Renevey, R. Delgado-Gonzalo, A. Lemkaddem, M. Proença, M. Lemay, J. Solà, A. Tarniceriu, and M. Bertschi, "Optical wrist-worn device for sleep monitoring," in *EMBEC & NBC 2017*, (Singapore), pp. 615–618, Springer Singapore, 2018.

[12] M. Pirhonen, M. Peltokangas, and A. Vehkaoja, "Acquiring respiration rate from photoplethysmographic signal by recursive bayesian tracking of intrinsic modes in time-frequency spectra," *Sensors (Basel)*, vol. 18, May 2018.

[13] P. Dehkordi, A. Garde, B. Molavi, J. M. Ansermino, and G. Dumont, "Extracting instantaneous respiratory rate from multiple photoplethysmogram respiratory-induced variations," *Frontiers in Physiology*, vol. 9, 2018.

[14] V. Chandel, J. Saha, C. Bhattacharyya, and A. Ghose, "Real-time robust estimation of breathing rate from ppg using commercial-grade smart devices: demo abstract," in *Proceedings of the 18th Conference on Embedded Networked Sensor Systems*, SenSys '20, (New York, NY, USA), pp. 633–634, Association for Computing Machinery, 2020.

[15] M. A. F. Pimentel, A. E. W. Johnson, P. H. Charlton, D. Birrenkott, P. J. Watkinson, L. Tarassenko, and D. A. Clifton, "Toward a robust estimation of respiratory rate from pulse oximeters," *IEEE Transactions on Biomedical Engineering*, vol. 64, no. 8, pp. 1914–1923, 2017.